ISSN 2070-0482, Mathematical Models and Computer Simulations, 2021, Vol. 13, No. 4, pp. 705–715. © Pleiades Publishing, Ltd., 2021.
Russian Text © The Author(s), 2020, published in Matematicheskoe Modelirovanie, 2020, Vol. 32, No. 12, pp. 114–128.

On Using Artificial Viscosity in Edge-Based Schemes on Unstructured Grids

P. A. Bakhvalov[a], * and T. K. Kozubskaya[a]

[a] *Keldysh Institute of Applied Mathematics, Russian Academy of Sciences, Moscow, Russia*

**e-mail: bahvalo@mail.ru*

Received June 17, 2020; revised June 17, 2020; accepted September 21, 2020

Abstract—When solving multidimensional problems of gas dynamics, finite-volume schemes using complete (i.e., based on a three-wave configuration) solvers of the Riemann problem suffer from shock-wave instability. It can appear as oscillations that cannot be damped by slope limiters, or it can lead to a qualitatively incorrect solution (carbuncle effect). To combat instability, one can switch to incomplete solvers based on a two-wave configuration near the shock wave, or introduce artificial viscosity. The article compares these two approaches on unstructured grids in relation to the EBR-WENO scheme for approximating convective terms and the classical Galerkin method for approximating diffusion terms. It is shown that the method of introducing artificial viscosity usually makes it possible to more accurately reproduce the flow pattern behind the shock front. However, on a three-dimensional unstructured grid, it causes dips ahead of the front, the depth of which depends on the quality of the grid, which can lead to an emergency stop of the calculation. Switching to an incomplete solver in this case gives satisfactory results with a much lower sensitivity to the quality of the mesh.

Keywords: edge-based scheme, unstructured mesh, artificial viscosity, carbuncle instability, WENO scheme

DOI: 10.1134/S2070048221040050

1. INTRODUCTION

For the numerical modeling of gas-dynamic flows with discontinuities, finite-volume schemes are most successfully used. The finite-volume scheme is characterized by three components: (1) a scheme for an approximate solution of the Riemann problem on the decay of a discontinuity to determine the flow through the face of a grid cell (hereinafter, for brevity, we will call it a solver); (2) by the reconstruction method, i.e., determining the values on the left and right on the face, supplied to the input to the solver; and (3) by the method of time integration. The schemes built within the finite-volume approach are conservative in construction: the stability and selection of a solution consistent with the entropy inequality is expected in practice due to the use of solvers. The calculation accuracy, characterized primarily by the value of the numerical dissipation, is determined by both the reconstruction method and the choice of the solver.

The most widely known is linear variable compensation with a slope limiter (see [1–3] and others). Since TVD constraints (constraints that ensure that the total variation of the solution when solving a scalar equation does not increase) lead to excessive numerical dissipation in the domain of a smooth solution, a combined approach is often used, in which the constraint is used only in part of the computational domain. Another, also well-known approach for determining the predisposed values is reconstruction based on ENO [4] (ENO with subgrid reconstruction [5], WENO [6–9], TENO [10, 11], and their numerous modifications). As a rule, their use provides correct computation in conjunction with any of the common solvers. All of these schemes, except ENO with subgrid reconstruction, naturally generalize to multidimensional Cartesian grids.

On an unstructured grid, the reconstruction of variables becomes much more complicated, although the basic approaches to modeling discontinuous solutions remain the same. Linear reconstruction with slope limiters was used in [12–14] for circuits with the definition of variables at the nodes and in [15, 16] with the definition of variables in the sense of the integral average over the grid element. WENO schemes with multidimensional polynomial reconstruction were studied in [17–21]. The schemes based on this

approach reproduce the unsteady flow behind the shock wave front better than others (in problems where it takes place), but they have an excessively high computational cost.

The EBR-WENO scheme [22, 23] is a synthesis of the technique of the quasi-one-dimensional reconstruction of variables on unstructured grids and a finite-difference WENO scheme (in the terminology of [8]) or a WENO class A scheme (in the terminology of [9]). Thus, it combines the relative simplicity with the low computational cost of schemes with linear reconstruction and the accuracy of finite-difference WENO schemes on uniform grids. Moreover, the EBR-WENO scheme allows the use of any solver.

In the one-dimensional case, the suppression of oscillations at the discontinuity is related almost exclusively to the choice of a suitable reconstruction method. However, in the multidimensional case and, moreover, on an unstructured grid, the use of a reconstruction that ensures the boundedness of the total variation of the solution for the scalar equation is no longer sufficient. Full solvers, that is, solvers based on the three-wave model (Godunov, Roe, HLLC flows), allow us to achieve better accuracy than incomplete ones based on the two-wave model (Lax–Friedrichs–Rusanov (LFR) flows, HLL); for a detailed description of all the listed solvers, see [24]. However, finite-volume schemes using full solvers suffer from shock-wave instability. This effect takes place even when using the basic scheme without reconstruction (or, which is the same, with the reconstruction of physical variables by a piecewise constant function), and even more so when using complex reconstructions such as WENO or EBR-WENO. Instability can manifest itself in the form of oscillations on shock waves that are not suppressed by the slope limiters, or lead to a qualitatively incorrect solution (carbuncle effect). To combat this effect, one can switch to incomplete solvers near the shock wave. This approach was proposed in [25], but the rule by which this switching is performed usually remained a tuning parameter.

An alternative approach to combat shock-wave instability was proposed by A.V. Rodionov [26, 27] and consists of introducing artificial viscosity in the form of an additional additive to molecular viscosity (and, together with this, to the coefficient of thermal conductivity). It is important that a formula is used for the viscosity coefficient that does not need to be adjusted for each new task.

This study continues the development of the EBR-WENO scheme. On two-dimensional and three-dimensional model problems, a comparison is made of the two methods described above for suppressing shock-wave instability, and the switch to incomplete solvers is carried out according to the same condition according to which this viscosity is introduced in the artificial viscosity method. The results are summarized in the conclusion section.

2. DESCRIPTION OF THE NUMERICAL METHOD

Throughout this study, the Euler equations are considered; the adiabatic exponent is 1.4. All the calculations are performed on tetrahedral grids and grid functions are defined at the nodes. Conservation laws are written for dual cells. The flow through the face of the dual cell is determined according to the Roe scheme [28] or the LFR scheme [29], into which the values of the characteristic variables reconstructed using the EBR-WENO method [22, 23] are substituted.

In the description of the calculations carried out below, one of the two approaches for suppressing the shock-wave's instability can be indicated. Switching to an incomplete solver means that the LF solver is used to calculate the flow between the control volumes of the nodes, at least one of which is in the vicinity of the shock wave, and in other cases the Roe flow is used. A node is considered to be in the vicinity of the shock wave if $\mathrm{div}\mathbf{u} + C_{th}\, a/l < 0$. The use of artificial viscosity and thermal conductivity means carrying out the calculation within the framework of the Navier-Stokes equations, and the coefficient of dynamic viscosity in the mesh node, in accordance with [26], is assumed to be

$$\mu_{AV} = (-0.5\rho l^2(\mathrm{div}\mathbf{u} + C_{th}\, a/l))_+. \tag{2}$$

Here ρ and a are the density and speed of sound in a node, l is the the local grid step (defined as the maximum height among all tetrahedra incident to this node). Index + means that μ_{AV} is assumed to be zero if the expression in parentheses is negative. Constant C_{th} is equal to 0.05, and the thermal conductivity coefficient is recalculated according to the viscosity coefficient based on the condition $\mathrm{Pr} = 0.72$. The diffusion terms are approximated by the classical Galerkin method with linear basis functions.

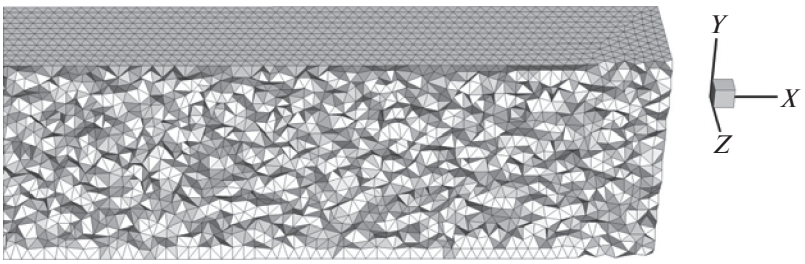

Fig. 1. Cleavage of the computational grid used in the calculation of the transfer of the shock wave.

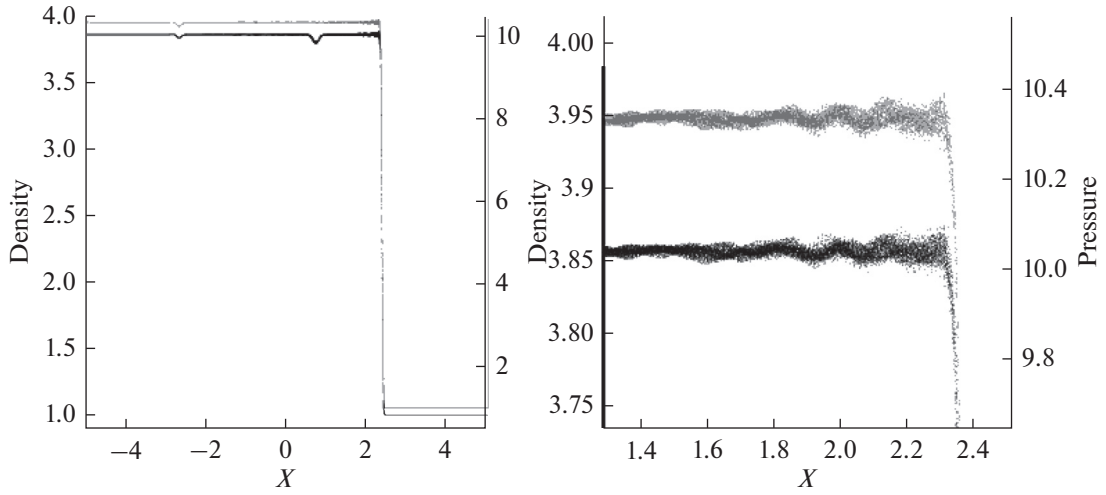

Fig. 2. General view of the shock wave (left) and an enlarged image of the graphs of density and pressure behind the front (right).

3. SHOCK WAVE PROPAGATION

Before proceeding to tests with a meaningful physical formulation, let us investigate how the scheme reproduces the propagation of a plane shock wave on an unstructured tetrahedral mesh. We will use an isotropic quasi-uniform mesh with the characteristic edge length $h = 1/40$. Its cleavage is shown in Fig. 1.

Let us set the initial data in the form of a shock wave with the Mach number M = 3, incident on the field ahead of the front $\rho_R = p_R = 1$, $\mathbf{u}_R = 0$. At the initial moment, the wave front coincides with the plane $x = -4$, the calculation is carried out before the time $t_{\max} = 1.8$.

The result of the calculation according to the EBR-WENO scheme with the Roe solver on an unstructured tetrahedral mesh is shown in Fig. 2. Each point corresponds to the value of the grid function at one grid point. The dips at $x \sim -2.7$ and at $x \sim -0.75$ are start-up errors, that is, waves arising from the smoothing of the initial wave profile by the numerical scheme, see [30, §15.8.4]. The first dip is an acoustic wave and the second dip is an entropy wave. These failures are inevitable and, at the same time, do not pose a problem for most applied problems.

Figure 2 shows that there are oscillations behind the shock front (which is typical for all high-precision schemes on unstructured grids). However, there are no numerical artifacts ahead of the shock front.

Let us investigate the appearance of numerical artifacts ahead of the shock front when the mesh quality deteriorates. To do this, we multiply the coordinates along the axes y and z of all grid nodes by coefficients h_y/h_x and h_z/h_x, respectively, and we leave the coordinate along the axis x unchanged. In Fig. 3 we will depict the dependence of the minimum density and minimum pressure on time for different h_y/h_x and h_z/h_x coefficients. The top row corresponds to scaling by only z; and the bottom one, to the same scaling by y and z. The Roe scheme was used to solve the discontinuity decay problem. It is seen that with an increase in anisotropy, density dips appear and grow.

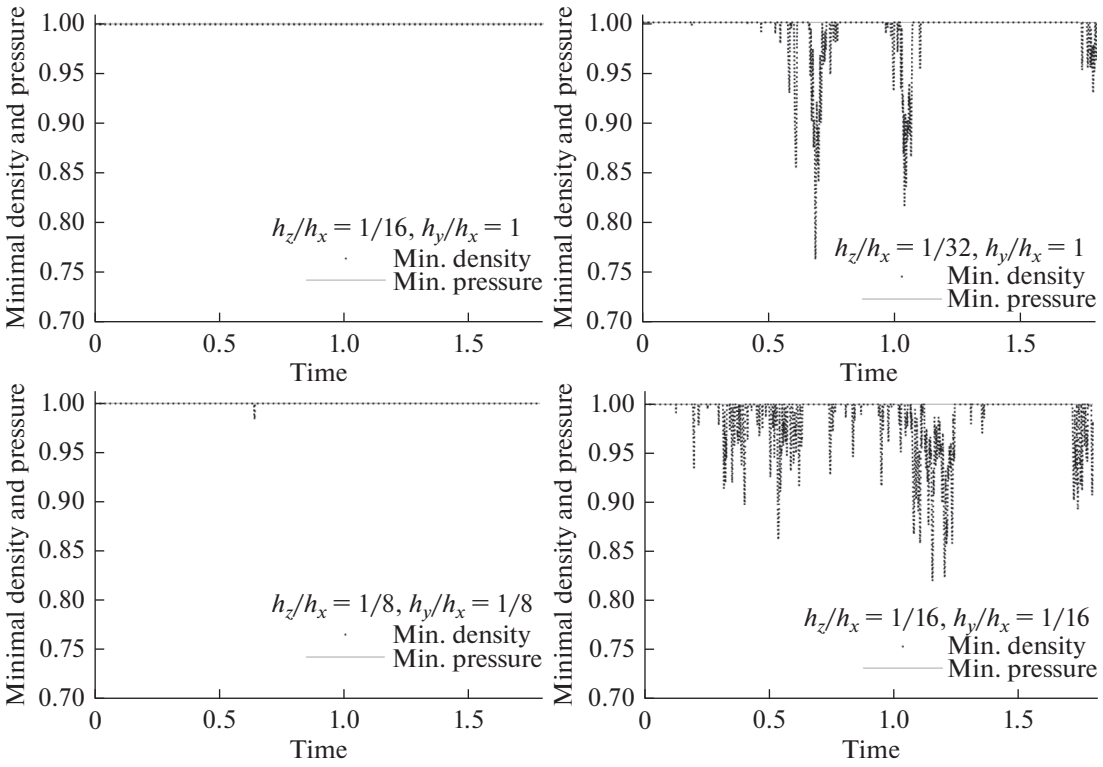

Fig. 3. Dependence of the minimum density and pressure for grids with different anisotropy coefficients in calculations without artificial viscosity.

Now let us carry out the same experiment, including artificial viscosity and thermal conductivity. The corresponding results when using the Roe and LF flows are shown in Fig. 4. It can be seen that dips appear in pressure and, to a lesser extent, in density, and this occurs at much lower anisotropy coefficients than in the absence of diffusion terms. The reason for this effect is that the approximation of the Laplace operator by the Galerkin method with piecewise linear basis functions does not satisfy the discrete maximum principle on a grid with obtuse-angled elements [31, Appendix E]. Note that when modeling high-Reynolds flows, this does not lead to problems in approximating diffusion terms, since the coefficients for them are small, including when using turbulence models. For stationary problems, presumably, it is possible to use the nonlinear approximation of the Laplacian, developed for the stationary convection-diffusion problem and monotonic on unstructured grids under very weak constraints on the shape of the elements [32, 33]; however, the possibility of using this method for nonstationary problems is unclear. A linear monotonic approximation of the Laplacian, as indicated in [32], is not known.

The appearance of time gaps seems to be random, since the position of the nodes of the unstructured mesh possesses this randomness. When scaling the mesh twice, these dips become clearly visible; with the further deterioration of the grid quality and/or an increase in the Mach number of the shock wave, these dips can reach negative pressure values and thus lead to an emergency stop of the calculation. Using an incomplete solver for the Riemann problem, as seen in Fig. 4 (left column), reduces the depth of the dips, but does not solve the problem.

Using a MinMod limiter instead of a WENO reconstruction avoids pressure dips for a much higher degree of anisotropy. The results using the Roe solver are shown in Fig. 5. When using the LF solver for meshes with $h_z/h_x = h_y/h_x = 1/8$, dips in density and pressure were observed only at $t < 0.01$, that is, during the period of smoothing of the initial profile of the shock wave.

4. SUPERSONIC FLOW AROUND A CYLINDER

In this and the next sections, we will consider two-dimensional problems on triangular meshes with almost no obtuse triangles. Since the approximation of the Laplacian by the classical Galerkin method with piecewise linear basis functions on grids without obtuse-angled elements is monotonic, the problems

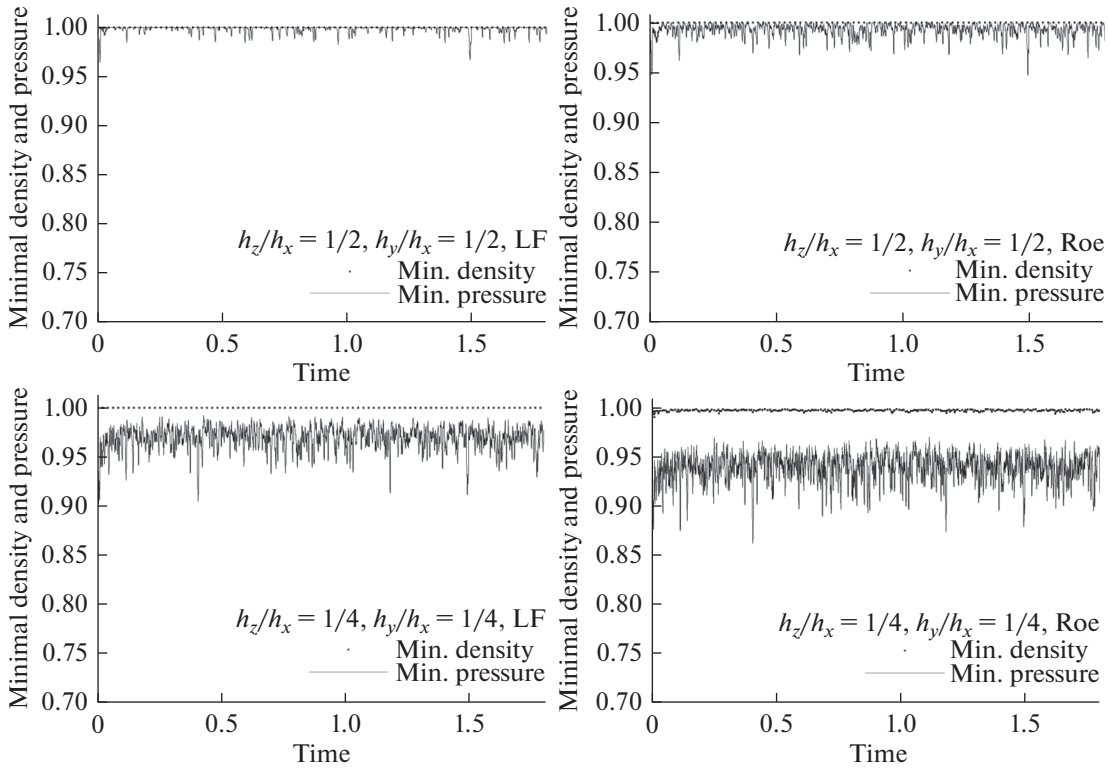

Fig. 4. Dependence of the minimum density and pressure for grids with different anisotropy coefficients in calculations with artificial viscosity and thermal conductivity.

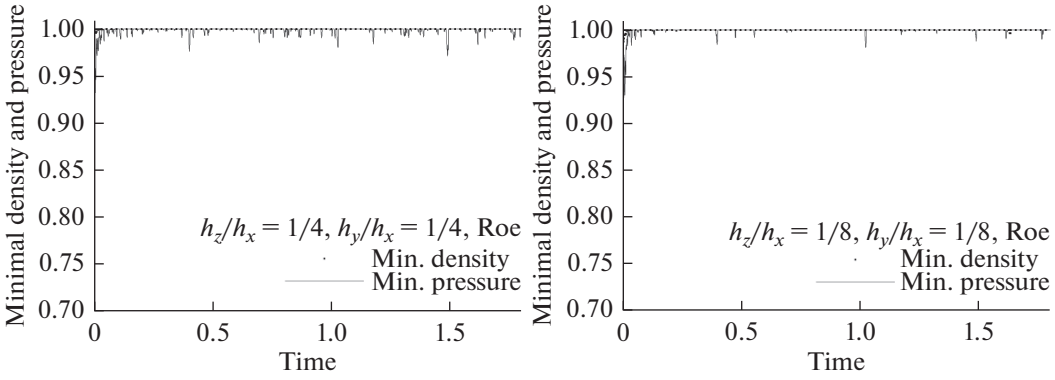

Fig. 5. Dependence of the minimum density and pressure for meshes with different anisotropy coefficients in calculations with artificial viscosity and thermal conductivity using the MinMod limiter.

described in the previous section do not arise. We compare two methods for suppressing shock-wave instability: switching to a two-wave solver and introducing artificial viscosity in the form of an addition to molecular viscosity.

WE consider a supersonic flow around a cylinder with the Mach number M = 3. The computational domain is set by the inequalities $1 < r < 3$ and $105° < \varphi < 255°$ and, as well as by a cover with an unstructured triangular mesh with a step of 0.026. The total number of triangles is 34016, of which 17 are obtuse.

Let us carry out the calculations with the following settings: (a) using the Roe solver without artificial viscosity; (b) the same with artificial viscosity; and (c) with a switch to the LFR solver in the vicinity of a shock wave without artificial viscosity. For each of the options, we will carry out calculations (1) according to the EBR-WENO scheme and (2) according to the EBR-WENO scheme with a switch to EBR-Min-

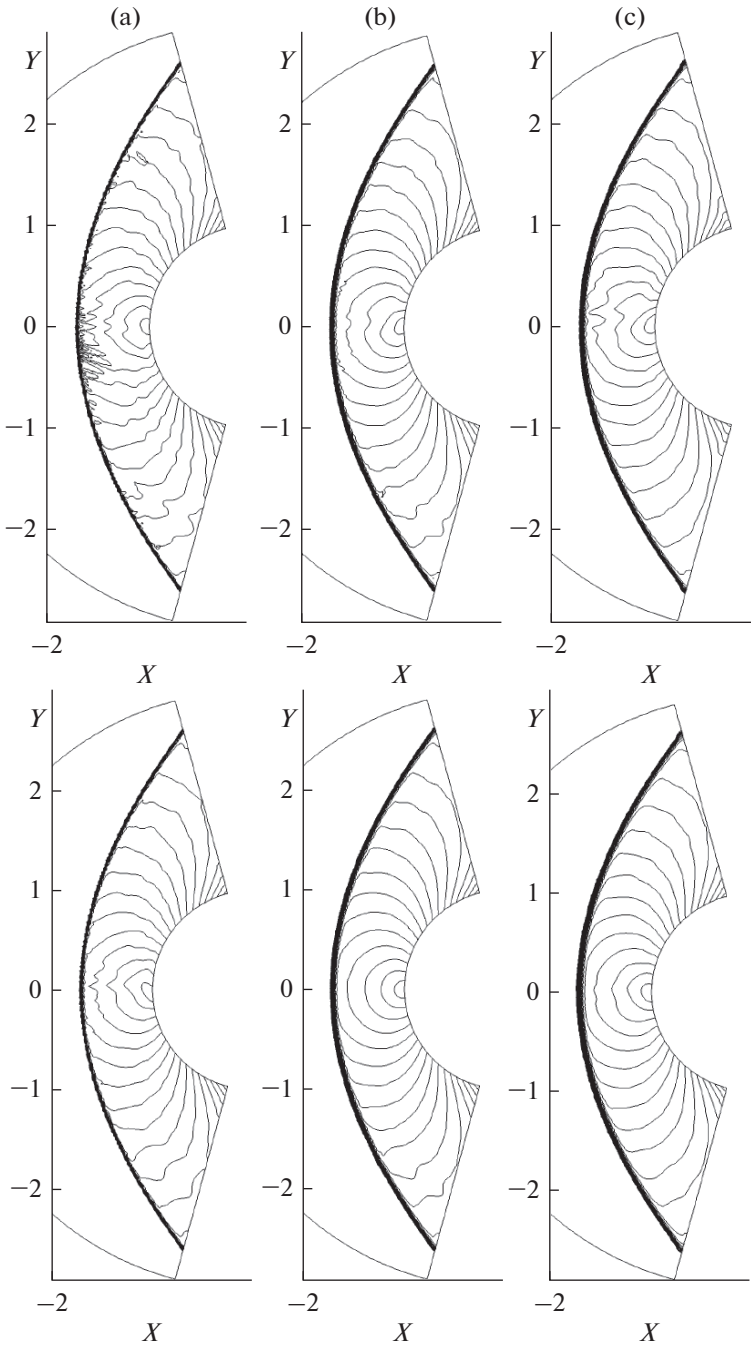

Fig. 6. Calculation results for the problem of supersonic flow around a cylinder: (a) Roe solver; (b) the same with artificial viscosity; (c) LFR solver without artificial viscosity. Top row: EBR-WENO scheme; bottom row: EBR-WENO circuit with a switch to MinMod in the vicinity of the shock wave.

Mod in the vicinity of the shock wave. The calculation results are summarized in Fig. 6, which shows 25 isolines of the local Mach number, ranging from 0.1 to 25 with a step of 0.1.

First of all, we note that the only calculation that converged to a stationary solution was the calculation with the introduction of artificial viscosity and aswitch to the MinMod limiter. Accordingly, the results of this calculation are the most accurate. The scheme with a switch to the MinMod limiter and an incomplete solver also gives an acceptable result. In the results of the other calculations, strong oscillations are observed.

Next, we will carry out calculations in the same geometry, but with the Mach number M = 10. The results of the calculations using the EBR-WENO scheme with a switch to EBR-MinMod in the vicinity

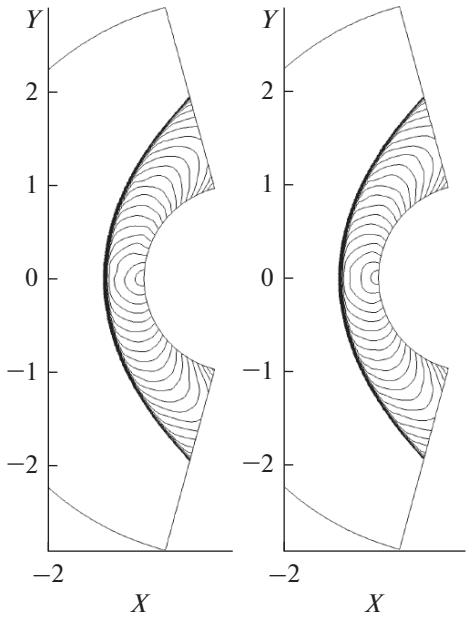

Fig. 7. Calculation results for the problem of supersonic flow around a cylinder at M = 10. EBR-WENO circuit with a switch to MinMod in the vicinity of the shock wave. Left: Roe solver with artificial viscosity; right: Roe solver with a switch to LFR solver, no artificial viscosity.

of the shock wave are shown in Fig. 7: on the left, using artificial viscosity; and on the right, with a switch to an incomplete solver in the vicinity of the shock wave. The third calculation, without suppressing the carbuncle-instability, ended with an emergency stop due to the occurrence of negative pressure. As with M = 3, the use of artificial viscosity gives a better result and allows us to achieve a stationary solution.

5. MACH DOUBLE REFLECTION PROBLEM

Let us now consider the problem of a double Mach reflection. Although the use of unstructured grids makes it possible to calculate this problem in a physical setting [34], we will use the classical setting [35]. The calculation is carried out in the area $0 < x < 3$, $0 < y < 1$. The initial data are set in the form of a shock wave, the front of which passes through the point (1/6, 0) and the normal to the front of which is rotated by 30 degrees clockwise relative to the X axis. The values ahead of the front (to the right of the front) are set equal to $\rho_R = 1.4$, $\mathbf{u}_R = 0$, and $p_R = 1$; and to the left of the front, equal to $\rho_L = 8$, $|\mathbf{u}_R| = 8.25$, and $p_R = 116.5$ ($\mathbf{u}_R$ is directed normal to the front). To avoid contamination of the solution by the parasitic wave arising from the rearrangement of the shock wave front under the grid profile, Rodionov's technique of is used [27]. At each time step, the values in all cells lying to the top left of all discontinuities and removed by more than $5l$ from them, for all physical variables, are kept equal to the exact solution for the shock wave in free space. An exact solution is also specified at the upper boundary of the computational domain.

The results of calculations on an unstructured mesh with the characteristic edge length $h = 1/240$ are shown in Fig. 8. Visually, both methods (the Roe solver with artificial viscosity and the Roe solver with a switch to the LFR solver without viscosity) give similar results. In particular, both approaches avoid the curvature of the Mach stem. A detailed examination shows that when switching locally to an incomplete solver, the head jump is slightly thicker.

For comparison, Fig. 9 shows the result of the calculation according to the EBR-MinMod scheme in the entire computational domain (Roe solver, with artificial viscosity). It can be seen that the vortex on the right side of the computational domain dissipated very strongly due to the numerical viscosity introduced by the MinMod limiter. This confirms the need to use more accurate reconstructions than the linear reconstruction with the MinMod limiter outside the vicinity of the shock wave.

6. SUPERSONIC FLOW AROUND A SPHERE

Let us turn to three-dimensional calculations and consider the problem of a supersonic flow around a sphere with the Mach number M = 10. The computational domain is set by the inequalities $1 < r < 1.8$,

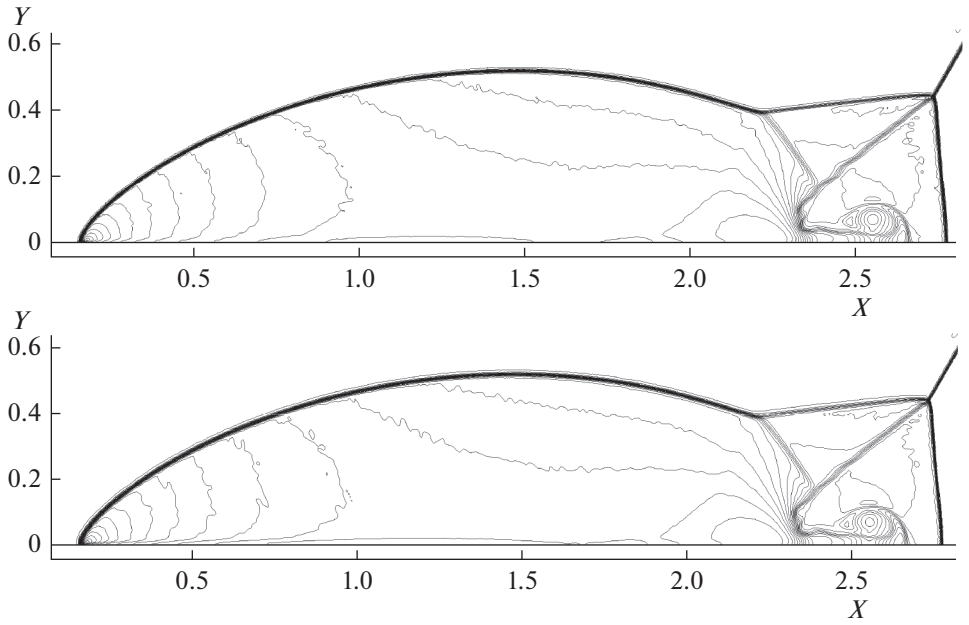

Fig. 8. Results of calculating the problem of double Mach reflection. EBR-WENO circuit with a switch to MinMod in the vicinity of the shock wave. Top: Roe artificial viscosity solver; bottom: Roe solver with a switch to LFR solver, no artificial viscosity.

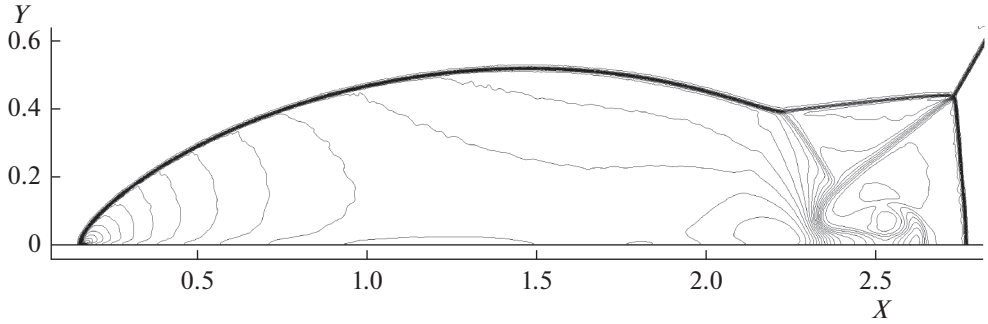

Fig. 9. Results of calculating the problem of double Mach reflection. EBR-MinMod.

$105° < \varphi < 255°$, where φ is the angle with the axis x. We cover an unstructured tetrahedral mesh with a step of 0.03 (coarse mesh), and we will also use a mesh obtained by grinding a coarse mesh (fine mesh). The total number of tetrahedra in the coarse mesh is 1185311, of which 485238 (41%) are obtuse-angled (i.e., such that the center of the circumscribed sphere lies outside the tetrahedron). The crushed mesh contains 9482488 tetrahedra, of which 3436878 (36%) are obtuse-angled.

Let us calculate this problem using the same schemes as the previous one. The results of the calculations in the section $z = 0$ are shown in Fig. 10.

It can be seen from Fig. 10 that, on a coarse mesh, the introduction of artificial viscosity made it possible to obtain a more symmetric flow pattern than switching to an incomplete solver of the Riemann problem. However, on a fine mesh, both schemes gave an asymmetrical picture. This result is consistent with the fact that on a coarse grid, only calculation (a) converged to a sufficiently small discrepancy. In calculations (b), (c), and (d), the result was visually established as shown in Fig. 10; however, persistent oscillations remained at the shock front. Presumably, these fluctuations, depending on the random arrangement of the nodes of the unstructured mesh, determine the observed asymmetry in the solution.

Let us also indicate the minimum pressure value for all grid nodes. In the calculations with a switch to an incomplete solver without using artificial viscosity, it did not fall below 0.9999 when using an explicit scheme in time and decreased with an increasing time step when using an implicit scheme. When using

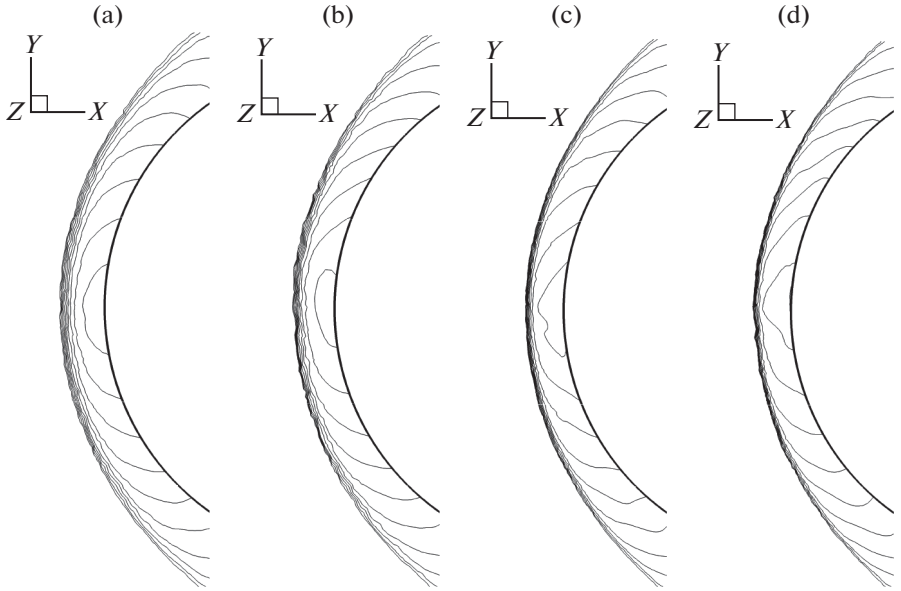

Fig. 10. Mach number isosurfaces in the central section for the problem of the flow around a sphere at M = 10. EBR-WENO scheme with switching to MinMod in the vicinity of the shock wave: (a) Roe solver with artificial viscosity; (b) switching to the LF solver, without artificial viscosity; (c) and (d) the same schemes on a fine mesh.

artificial viscosity and the Roe solver, it weakly depended on the Courant number and was approximately 0.948 on a coarse grid and 0.886 on a refined grid. With the simultaneous use of artificial viscosity and switching to an incomplete solver, the minimum pressure on the refined mesh is approximately 0.997.

7. CONCLUSIONS

In this study, two methods of suppressing shock-wave instability were considered, namely, the introduction of artificial viscosity on the shock wave and local switching to an incomplete solver of the Riemann problem. These methods are compared in relation to the EBR-WENO scheme for approximating convective fluxes and the Galerkin method with piecewise linear basis functions for approximating the diffusion terms on unstructured triangular and tetrahedral meshes. Both methods successfully suppress shock-wave instability, but exhibit different properties.

On grids of acute-angled triangles, the introduction of artificial viscosity is preferred. However, on the grids containing obtuse-angled elements, violation of the discrete maximum principle for the discrete Laplace operator can lead to the appearance of dips ahead of the shock front. These dips deepen as the mesh quality deteriorates. They can cause additional numerical oscillations, and when negative values are reached, an emergency stop of the counting. When switching in the shock wave zone from the WENO reconstruction to the MinMod limiter, the depth of the holes decreases significantly.

The method of switching to an incomplete solver of the Riemann problem on grids without obtuse-angled elements is inferior in quality to the method of introducing artificial viscosity. However, it is much less sensitive to mesh quality and thus more reliable. The sensor used in [26, 27] to determine the coefficient of artificial viscosity is suited for determining the zone in which switching to an incomplete solver of the Riemann problem should be performed.

Also, for the EBR-WENO scheme, the importance of switching to the use of the MinMod limiter in the shock wave zone was confirmed, as well as, vice versa, the importance of using a high-precision reconstruction outside the vicinity of the front.

FUNDING

This study was financially supported by the Russian Science Foundation (project 20-41-09018).

REFERENCES

1. V. P. Kolgan, "Application of the principle of minimizing the derivative to the construction of finite-difference schemes for computing discontinuous solutions of gas dynamics," J. Comput. Phys. **230** (7), 2384–2390 (2011).
2. A. V. Rodionov, "Monotonic scheme of the second order of approximation for the continuous calculation of non-equilibrium flows," USSR Comp. Math. Math. Phys. **27** (2), 175–180 (1987).
3. B. van Leer, "Towards the ultimate conservative difference scheme. V. A second-order sequel to Godunov's method," J. Comput. Phys. **32** (1), 101–136 (1979).
4. A. Harten and S. Osher, "Uniformly high-order accurate essentially nonoscillatory scheme. I," SIAM J. Numer. Anal. **24** (2), 279–309 (1987).
5. A. Harten, "ENO schemes with subcell resolution," J. Comput. Phys. **83** (1), 148–184 (1989).
6. X.-D. Liu, S. Osher, and T. Chan, "Weighted essentially non-oscillatory schemes," J. Comput. Phys. **115** (1), 200–212 (1994).
7. G.-S. Jiang and C.-W. Shu, "Efficient implementation of weighted ENO schemes," J. Comput. Phys. **126** (1), 202–228 (1996).
8. C.-W. Shu, "Essentially non-oscillatory and weighted essentially non-oscillatory schemes for hyperbolic conservation laws," ICASE Report No. 97-65 (NASA Langley Research Center, Hampton, VA, 1997); in *Advanced Numerical Approximation of Nonlinear Hyperbolic Equations*, Ed. by A. Quarteroni, Lecture Notes in Mathematics (Springer, Berlin, 1998), Vol. 1697, pp. 325–432.
9. R. Zhang, M. Zhang, and C.-W. Shu, "On the order of accuracy and numerical performance of two classes of finite volume WENO schemes," Commun. Comput. Phys. **9** (3), 807-827 (2011).
10. L. Fu, X. Y. Hu, and N. A. Adams, "A family of high-order targeted ENO schemes for compressible-fluid simulations," J. Comput. Phys. **305**, 333–359 (2016).
11. L. Fu, X. Y. Hu, and N. A. Adams, "Targeted ENO schemes with tailored resolution property for hyperbolic conservation laws," J. Comput. Phys. **349**, 97–121 (2017).
12. T. J. Barth and D. C. Jespersen, "The design and application of upwind schemes on unstructured meshes," in *27th Aerospace Science Meeting* (Reno, NV, January 9–12, 1989), AIAA Paper 89-366 (1989).
13. L. Fezoui and B. Stouffet, "A class of implicit schemes for Euler simulations with unstructured meshes," J. Comput. Phys. **84** (1), 174–206 (1989).
14. H. Luo, J. D. Baumt, and R. Lohner, "Edge-based finite element scheme for the Euler equations," AIAA J. **32** (6), 1183-1190 (1994).
15. H. Jasak, H. G. Weller, and A. D. Gosman, "High resolution NVD differencing scheme for arbitrarily unstructured meshes," Int. J. Numer. Methods Fluids **31** (2), 431–449 (1999).
16. C. Le Touze, A. Murrone, and H. Guillard, "Multislope MUSCL method for general unstructured meshes," J. Comput. Phys. **284**, 389–418 (2015).
17. W. R. Wolf and J. L. F. Azevedo, "High-order ENO and WENO schemes for unstructured grids," Int. J. Numer. Methods Fluids **55** (10), 917–943 (2007).
18. M. Dumbser, M. Käser, V. A. Titarev, and E. F. Toro, "Quadrature-free non-oscillatory finite volume schemes on unstructured meshes for nonlinear hyperbolic systems," J. Comput. Phys. **226** (1), 204–243 (2007).
19. P. Tsoutsanis, V. A. Titarev, and D. Drikakis, "WENO schemes on arbitrary mixed-element unstructured meshes in three space dimensions," J. Comput. Phys. **230** (4), 1585–1601 (2011).
20. Y. Liu and Y.-T. Zhang, "A robust reconstruction for unstructured WENO schemes," J. Sci. Comput. **54** (2–3), 603–621 (2013).
21. P. Tsoutsanis, A. F. Antoniadis, and D. Drikakis, "WENO schemes on arbitrary unstructured meshes for laminar, transitional and turbulent flows," J. Comput. Phys. **256**, 254–276 (2014).
22. P. A. Bakhvalov and T. K. Kozubskaya, "EBR-WENO scheme for solving gas dynamics problems with discontinuities on unstructured meshes," KIAM Preprint No. 23 (Keldysh Inst. Appl. Math., Moscow, 2017) [in Russian].
23. P. Bakhvalov and T. Kozubskaya, "EBR-WENO scheme for solving gas dynamics problems with discontinuities on unstructured meshes," Comput. Fluids **157**, 312–324 (2017).
24. E. F. Toro, *Riemann Solvers and Numerical Methods for Fluid Dynamics: A Practical Introduction* (Springer, Berlin, 1997).
25. J. J. Quirk, "A contribution to the great Riemann solver debate," Int. J. Numer. Methods Fluids **18** (6), 555–574 (1994).
26. I. Yu. Tagirova and A. V. Rodionov, "Application of the artificial viscosity for suppressing the carbuncle phenomenon in Godunov-type schemes," Math. Models Comput. Simul. **8** (3), 249–262 (2016).
27. A. V. Rodionov, "Artificial viscosity to cure the shock instability in high-order Godunov-type schemes," Comput. Fluids **190**, 77–97 (2019).
28. P. L. Roe, "Approximate Riemann solvers, parameter vectors, and difference schemes," J. Comput. Phys. **43** (2), 357–372 (1981).

29. V. V. Rusanov, "The calculation of the interaction of non-stationary shock waves and obstacles," USSR Comput. Math. Math. Phys. **1** (2), 304–320 (1962).
30. R. J. LeVeque, *Finite Volume Methods for Hyperbolic Problems* (Cambridge University Press, Cambridge, 2002).
31. H. Nishikawa, "Beyond interface gradient: A general principle for constructing diffusion schemes," in *40th Fluid Dynamics Conference and Exhibit* (Chicago, IL, June 28 – July 1, 2010), AIAA Paper No. 2010-5093 (2010).
32. K. Lipnikov, M. Shashkov, D. Svyatskiy, and Yu. Vassilevski, "Monotone finite volume schemes for diffusion equations on unstructured triangular and shape-regular polygonal meshes," J. Comput. Phys. **227** (1), 492–512 (2007).
33. K. Lipnikov, D. Svyatskiy, and Yu. Vassilevski, "Minimal stencil finite volume scheme with the discrete maximum principle," Russ. J. Numer. Anal. Math. Modell. **27** (4), 369–385 (2012).
34. U. S. Vevek, B. Zang, and T. H. New, "On alternative setups of the double Mach reflection problem," J. Sci. Comput. **78** (2), 1291–1303 (2019).
35. P. Woodward and P. Colella, "The numerical simulation of two-dimensional fluid flow with strong shocks," J. Comput. Phys. **54** (1), 115–173 (1984).

SPELL: 1. OK